BRAIN CONNECTIVITY
Volume 4, Number 4, 2014

DOI: 10.1089/brain.2014.0225

Functional Magnetic Resonance Imaging Networks Induced by Intracranial Stimulation May Help Defining the Epileptogenic Zone

Stephen E. Jones,[1] Myron Zhang,[1] Rafi Avitsian,[2] Pallab Bhattacharyya,[1] Juan Bulacio,[3] Fernando Cendes,[4] Rei Enatsu,[3] Mark Lowe,[1] Imad Najm,[3] Dileep Nair,[3] Michael Phillips,[1] and Jorge Gonzalez-Martinez[3]

Abstract

Patients with medically intractable epilepsy often undergo invasive evaluation and surgery, with a 50% success rate. The low success rate is likely due to poor identification of the epileptogenic zone (EZ), the brain area causing seizures. This work introduces a new method using functional magnetic resonance imaging (fMRI) with simultaneous direct electrical stimulation of the brain that could help localize the EZ, performed in five patients with medically intractable epilepsy undergoing invasive evaluation with intracranial depth electrodes. Stimulation occurred in a location near the hypothesized EZ and a location away. Electrical recordings in response to stimulation were recorded and compared to fMRI. Multiple stimulation parameters were varied, like current and frequency. The brain areas showing fMRI response were compared with the areas resected and the success of surgery. Robust fMRI maps of activation networks were easily produced, which also showed a significant but weak positive correlation between quantitative measures of blood-oxygen-level-dependent (BOLD) activity and measures of electrical activity in response to direct electrical stimulation (mean correlation coefficient of 0.38 for all acquisitions that produced a strong BOLD response). For four patients with outcome data at 6 months, successful surgical outcome is consistent with the resection of brain areas containing high local fMRI activity. In conclusion, this method demonstrates the feasibility of simultaneous direct electrical stimulation and fMRI in humans, which allows the study of brain connectivity with high resolution and full spatial coverage. This innovative technique could be used to better define the localization and extension of the EZ in intractable epilepsies, as well as for other functional neurosurgical procedures.

Key words: connectivity; direct intracranial stimulation; functional MRI; intracranial EEG; intracranial electrodes; intractable epilepsy

Introduction

A major impediment to the complete cure of pharmacologically resistant focal epilepsies is the insufficient identification of the epileptogenic zone (EZ) and related epileptic network. Better definition of the localization and extent of the EZ could aid thousands of patients with pharmacoresistant seizures (Berg, 2009; Berg and Kelly, 2006; Brodie et al., 2005; Kwan and Brodie, 2000; Sillanpää and Schmidt, 2006). Several techniques currently exist for studying brain connectivity. Among these, cortico-cortical evoked potentials (CCEPs) use direct electrical stimulation and recording of intracranial electrodes to study electrophysiological connectivity within the brain (Matsumoto et al., 2004, 2007). With this technique, a pulse of current is sent through a pair of electrode contacts, and the voltage response is recorded at other contacts. CCEPs may be used to help identify the EZ and epileptic networks to guide resective surgery in patients with pharmacoresistant seizures (Iwasaki et al., 2010). The weakness of intracranial electrode recordings, however, is incomplete spatial coverage and imprecise localization of source signals. In contrast, the blood-oxygen-level-dependent (BOLD) response of functional magnetic resonance imaging (fMRI) can be used to reveal localized networks of activity throughout the entire brain, typically through task-related activation or while the patient is in the resting state (Logothetis, 2012). This study combines these methods to investigate the BOLD response to direct

[1]Imaging Institute, [2]Anesthesia Institute, and [3]Epilepsy Center, Cleveland Clinic, Cleveland, Ohio.
[4]Department of Neurology, University of Campinas–UNICAMP, Campinas, Brazil.

intracranial electrical stimulation of the human brain (termed DES-fMRI) and to compare this response to evoked electrical recordings from other intracranial electrodes. All measurements occurred in patients with pharmacoresistant seizures undergoing routine invasive presurgical evaluation comprising placement of multiple stereotactic electroencephalogram (SEEG) depth electrodes.

Earlier studies of DES-fMRI assessed patients with Parkinson's disease during deep-brain stimulation of the basal ganglia but did not compare fMRI activity to measures of electrical activity (Hesselmann et al., 2004; Jech et al., 2001; Phillips et al., 2006; Stefurak et al., 2003). Comparable studies in animals (Angenstein et al., 2007; Matsui et al., 2011; Tolias et al., 2005) have typically not included comparisons of fMRI to electrical activity or have focused on the comparison in a specific region of the brain as opposed to broader network activation. In contrast, each of our patients is implanted with up to 15 depth electrodes, each containing up to 12 contacts, which allows for a more complete and three-dimensional comparison of electrophysiology networks to fMRI patterns throughout the entire brain. In this study, we aimed to compare the spatial activation patterns and strengths of the simultaneously acquired DES-fMRI BOLD response to SEEG recordings throughout the brain. We also investigated how various parameters, including stimulation frequency, stimulation current, and presence of an EZ, affect the DES-fMRI BOLD response. This research presents preliminary data from a new technique for studying brain connectivity that could enhance the preoperative identification of epileptic areas in the human brain.

Materials and Methods

Patient selection and flow

The study population included eight patients with pharmacoresistant seizures who were already undergoing an invasive evaluation for presurgical planning using the SEEG methodology. The recommendations for SEEG implantation as well as the general planning of electrode sites were made during our weekly Epilepsy Center multidisciplinary patient management conference following detailed review and discussion of results of the noninvasive localization methods (and at times previous invasive tests and other surgical procedures). In addition to the general criteria used for invasive extraoperative monitoring, additional specific criteria for the selection of SEEG included the following: (1) possible deep-seated location of the EZ, (2) the need for extensive bi-hemispheric explorations, and (3) presurgical evaluation suggestive of a functional network involvement (e.g., limbic system).

On the day before explantation, enrolled patients underwent an extensive CCEP study focusing on stimulation of the SEEG contact pair best colocalized with the presumptive EZ, in addition to control stimulations of non-EZ contacts in proximal and distal regions along the same electrode. The signature portion of this study occurred during the explantation procedure, within an intraoperative MRI suite (IMRIS) and while the patient was under general anesthesia. Before the first explantation was initiated, the previous CCEP study was repeated to document the effects of used anesthetics. For safety reasons, we were not comfortable with performing MRI with more than one electrode implanted. Therefore, the explantation proceeded, with sequential removal of all electrodes except for the one with contacts closest to the hypothesized EZ. The MRI scanner was then brought over the operating table and DES-fMRI was performed, as detailed later in ''Magnetic resonance imaging'' section. After imaging, the final electrode was removed, and patients were emerged from general anesthesia and transported to the Post Anesthesia Care Unit (PACU) in stable condition. All patients were subsequently discharged with resections of the EZ performed about 2–3 months later (routine practice to minimize infection). Note that these resections were planned solely using routine clinical considerations, and were not affected by the results of this study. IRB approval was obtained and HIPPA standards were strictly followed for this study.

Safety testing

The primary safety concern with this imaging procedure is resistive joule heating caused by radiofrequency (RF) coupling with conducting parts of the implant. The degree of heating is heavily dependent on the configuration and location of the conductor, grounding, RF pulse sequence, magnetic field strength, and RF coil used. The complexities of these variables preclude reliable simulation for prediction of heating; thus, phantom testing was used to assess potential heating problems. This methodology has routinely been used to assess heating effects in other studies (Baker et al., 2004, 2006; Rezai et al., 2002).

End-to-end phantom testing was conducted within the same IMRIS, using the same configuration of receive-only phased array coil, intracranial electrodes, connectors, and stimulation hardware. The phantom itself comprised a head-torso-shaped container with polyacrylic gel, which has similar dielectric properties as human tissues. A single electrode was inserted into the container in a fashion similar to the human insertion, and Fluoroptic temperature sensors (model m3300; Luxtron) were placed adjacent to the surfaces of multiple contacts. Real-time heating was recorded during full acquisitions of T1-weighted multiplanar gradient-recalled (MPGR), T2-weighted fast single-echo (FSE), localization, and echo-planar imaging (EPI) sequences. Numerous configurations were tested, including variations in cable location and orientation, cable lengths, various disconnections, and grounding patterns.

Cortico-cortical evoked potentials

CCEP data were gathered by stimulating a pair of adjacent contacts and recording all remaining contacts (typically between 100 and 200 contacts). Each recording contact measures the evoked potential localized to the area around the contact. Stimulation, which used current-controlled Grass Technologies S88 and SUI-7 units (Astro-Med) located outside the MRI scanner in the control room, was performed at 1 Hz for $\sim$45 sec, with alternating unipolar 0.3-msec square wave pulses, at currents between 4 and 15 mA. These parameters are typical for clinical stimulation during invasive evaluations, whose physiological effect can range from excitation to dysfunction depending on the current magnitude or frequency (Gordon et al., 1990; Lesser, 1987). Note that a minimum current of about 1 mA is required for sensory or motor response at 25 Hz. An optical current isolator was

used to ensure the patient did not share a common ground with the MRI scanner. The forty-five 1-sec periods recorded at each contact were then averaged to produce a mean waveform over 1 sec.

The measure of electrophysiological connectivity used to compare with fMRI was the root mean square of this mean waveform in the 50-msec period after the stimulation pulse. This period was used to score the CCEPs because it encompasses the typical time range in which the initial voltage response occurs (Matsumoto et al., 2004, 2007). Other commonly used measures for CCEP response strength include peak-to-peak amplitudes in the waveform (Matsumoto et al., 2004, 2007), which is compared to the root mean square measure. Figure 1 shows an example of a recorded CCEP waveform and some features used to score response strength.

CCEPs were recorded outside the MRI scanner the day before imaging (patient awake). For two patients, CCEPs were also recorded on the day of imaging (patient under general anesthesia) to compare with the CCEPs without anesthesia. The CCEPs recorded with the patient awake were the ones used in comparisons with fMRI. The particular target electrode contacts for stimulation were those closest to the hypothesized EZ (within tissue planned for subsequent resection) as well as a control stimulation using another pair of electrode contacts distal to the EZ along the same electrode, typically those most lateral or medial to EZ contacts.

Magnetic resonance imaging

All electrodes were removed, except for the one with contacts closest to the hypothesized EZ, in an IMRIS (using 1.5 T Siemens Espree with receive-only split array head coil). After safety checklists were reviewed, the MRI scanner was brought over the patient and imaging commenced with an anatomical scan using an MPGR (TR/TE/FA 11 msec/4.6 msec/20°; acquisition matrix 256×256; 1-mm isotropic voxels). This was followed by four or five acquisitions of DES-fMRI using an EPI sequence (2000 msec/50 msec/80°; acquisition matrix 64×64; 7-mm slice thickness with 2-mm gap; $4 \times 4\,mm^2$ in-plane voxel size).

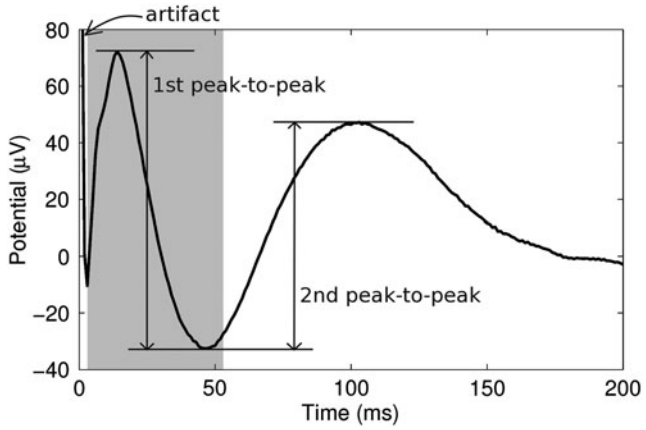

FIG. 1. Illustration of how cortico-cortical evoked potentials (CCEPs) were scored. The scalar CCEP score used for comparison against functional magnetic resonance imaging (fMRI) was the root-mean-square of the waveform in a 50-msec window (shaded region) following the end of the stimulus artifact. Other commonly used CCEP scores are the peak-to-peak amplitudes of the first and second deflections, also indicated in the figure.

Each fMRI run used a block design, with four cycles of 32 sec of electrical stimulation followed by 32 sec of no stimulation. Stimulation parameters were based on our previous experience with brain stimulation for CCEPS (Matsumoto et al., 2004, 2007). Electrical stimulation was performed at 20 Hz, with 0.3-msec square wave pulses. During each 32-sec block of stimulation, there was 1 sec of rest every 8 sec to avoid current limitations for tissue damage (Gordon et al., 1990; Jayakar, 1993). Each patient typically underwent four EPI acquisitions that included stimulation of the hypothesized EZ and the control non-EZ (as defined by the extraoperative SEEG monitoring phase), each at a low current (4 mA) and a high current (8 or 15 mA). These values for current were chosen to match typical stimulation currents used in CCEPs (Matsumoto et al., 2004, 2007). Stimulation was varied to 1, 5, and 10 Hz in some patients to observe the effect of frequency. Due to time considerations, we did not perform low-current stimulations in patients in which frequency was varied. In three patients, we also used an event stimulation design, which was successful in one patient when the stimulation duration was increased from 1 to 2 sec (followed by 11 sec of rest, then repeated for the duration of the MRI [300 sec]; 8 mA; 40 Hz). The other two patients using an event design with stimulation over a 1-sec duration showed weak but positive activation, and are not presented. Throughout all the procedures (pre-explantation CCEPs, explantation, and imaging), the patient remained under general anesthesia, detailed later in ''Anesthesia'' section, with a respiration rate fixed at one breath per 6 sec.

fMRI analysis

fMRI analysis used Analysis of Functional NeuroImages (AFNI) 3ddeconvolve (Cox and Hyde, 1997) and included removal of the first five volumes, slice timing correction, motion correction, Gaussian blur (4-mm full-width at half-maximum), scaling each voxel to a common mean, and ordinary least-squares linear regression against a model hemodynamic response function and polynomial (degree 3) baselines. The resulting t-statistic from the regression was used as the measure of fMRI activation in each voxel, with sample sizes of 155 (160 – 5 MRI volumes).

Activation maps were produced using MATLAB (MathWorks, Inc.) and used a significance threshold of $p < 0.01$, which corresponded to $|t| > 2.6$. Clustering was also applied, with six-neighbor clusters of activation smaller than 10 voxels discarded. fMRI t-values were compared against CCEP scores by registering the location of each CCEP electrode contact to an MRI voxel. Coordinates of CCEP electrode contacts were identified from a thin-section anatomic CT scan obtained following implantation of electrodes. This anatomical scan was then registered to the MPGR anatomical scan done in the IMRIS (with the patient in the same orientation as for the fMRI scans). Finally, the MPGR scan was registered to an fMRI EPI volume, and the two transformation matrices were concatenated and applied to the CCEP coordinates. All image registration was affine and was performed using FSL FLIRT (Jenkinson and Smith, 2001;

Jenkinson et al., 2002). Comparison of fMRI *t*-values and CCEP scores in coregistered electrode contact locations used the Pearson's product-moment correlation coefficient. The resulting *p* value was calculated with the ''corrcoef'' function in MATLAB, with the assumption that the data have a multivariate normal distribution. To account for uncertainties in registration, the volume of *t*-values was spatially smoothed using a Gaussian filter ($\sigma = 0.65$) over $3 \times 3 \times 3$ voxels before being correlated with CCEP scores.

Anesthesia

DES-fMRI was performed under general anesthesia with endotracheal intubation and mechanical ventilation, under the design and supervision of a neuro-anesthesiologist (R.A.), with the goal of minimizing inhibitory effects. Induction of general anesthesia was achieved with intravenous Propofol in three cases, Etomidate in one, and Ketamine with the fifth patient. Muscle relaxation was provided for all cases using rocuronium. All patients received intravenous Ketamine infusion as part of their anesthetic maintenance. Ketamine was chosen for its less inhibitory and in fact epileptogenic effect in patients with a history of seizures (Modica et al., 1990). Ketamine dose varied in two patients receiving low dose (7–10 and 15) and two patients with a higher dose (50–60) mcg/(kg·min^{-1}). Volatile anesthetic (Isoflurane or Sevoflurane) was used at around 0.5 Minimum Alveolar Concentration for all patients. At the end of the procedure all patients were extubated and transported to PACU in stable condition. Note that CCEPs were performed twice on patients, with and without anesthesia, to estimate the effects of the anesthesia on brain responses.

Results

Safety

Heating was negligible during phantom testing (i.e., < 1°C) for a completely connected cable exiting superiorly from the head and routed near the central axis of the bore and for T1-MPGR and EPI sequences. Outside of these parameters, heating up to 6°C was recorded; the greatest temperature increase occurred with the use of a T2-FSE sequence with disconnected cables lying along the floor of the bore. This sequence was not used in human scans and was included in the safety testing only to confirm that thermometry could record temperature changes from sequences with a high specific absorption rate. Finally, following subsequent resection of the epileptogenic tissue that surrounded the stimulating electrode contacts during the fMRI experiment, a dedicated qualitative evaluation by a neuropathologist showed no thermal damage on low-power H&E stain, as would be evidenced by necrosis or nuclear streaming. The only pathology visible was expected microhemorrhage and edema due to the insertion and presence of the electrode.

Network BOLD activation

A total of eight patients underwent DES-fMRI, of which the first three were stimulated at 1 Hz during fMRI and showed insignificant BOLD response. The subsequent five patients were stimulated at higher frequencies and all showed robust BOLD responses. Table 1 gives a clinical overview for each of these five patients (termed P1 through

TABLE 1. CLINICAL INFORMATION ON THE FIVE SUCCESSFUL STUDY SUBJECTS

Patient ID[a]	*Age (years)*	*Duration of epilepsy (years)*	*Gender*	*Dominance*	*Epilepsy type*	*Type of seizures*	*Type of resection*	*Pathology*	*Seizure outcome (Engel)*
P1	25	17	F	Right	Left focal	Complex motor	Left posterior orbitofrontal, left pars orbitalis, left temporal pole	MCD	I
P2	41	25	F	Right	Right focal	Complex partial → generalized tonic-clonic	Right mid-posterior cingulate gyrus	MCD	I
P3	42	14	F	Right	Right focal	Somatosensory aura → complex partial	Right temporal lobectomy	MCD	IV
P4	64	14	M	Left	Right focal	Dialeptic	Right frontal lobectomy	MCD	I
P5	54	24	F	Right	Right focal	Automotor → left clonic → generalized tonic-clonic	Right orbitofrontal and temporal	MCD	N/A[b]

[a]The first three patients performed at 1 Hz showed no activation, are not enumerated, and not included in this table.
[b]Six-month outcome not available at the time of this writing.
MCD, malformations of cortical development.

Table 2. Overview of All Direct Electrical Stimulation–Functional Magnetic Resonance Imaging Results Obtained from Five Patients

Patient ID	*Figure no.*	*Stim. location*	*Stim. frequency (Hz)*	*Stim. current (mA)*	*CCEP correlation (r, p)*	*BOLD response*	*Resected*	*Seizure free*
P1	2A	Left orbitofrontal	20	15	0.44, 1.6×10^{-5}	Local, network (strong)*	Yes	Yes
	2B	Left forceps minor	20	15	N/A[a]	Local, network (strong)	No	
	2C	Left frontal white matter	20	15	N/A[a]	None	No	
P2	2D	Right posterior cingulate	20	8	0.28, 0.029	Local, network (strong)*	Yes	Yes
	3A		20	4	0.084, 0.52	Local, network (strong)		
	2E	Right supramarginal gyrus	20	8	-0.36, 4.4×10^{-3}	Local (weak)	No	
	3B		20	4	0.017, 0.89	Network (weak, negative)		
P3	2F	Right insula	20	8	0.54, 2.8×10^{-9}	Local, network (strong)*	No	No
	3C		20	4	0.49, 8.7×10^{-8}	Local, network (strong)		
	2G	Right superior temporal gyrus	20	8	0.029, 0.76	Local (weak)	Yes	
	3D		20	4	0.22, 0.024	None		
P4	2H	Right medial orbitofrontal	20	8	0.47, 5.2×10^{-5}	Local (strong)*	Yes	Yes
	2I	Right pars orbitalis	20	8	0.10, 0.43	Local (weak)	Yes	
	3E		10	8	0.24, 0.060	None		
	3F		5	8	-0.094, 0.45	None		
P5		Right prefrontal	20	8	N/A[b]	Distal (putamen, strong)	No	N/A[c]
	9	Right operculum	20	8	N/A[b]	Strong local and distal	Yes	
			20	1	N/A[b]	Negligible		
	9		20[d]	8	N/A[b]	Strong local and distal		
	Supplementary Video S1		40[b]	4				

Supplementary Data are available online at www.liebertpub.com/brain
[a]P1 only had CCEPs performed at the left orbitofrontal contacts.
[b]P5 CCEP correlations are not available due to technical failure during acquisition.
[c]Outcome results are not available at the time of this writing.
[d]Event design.
*These high-current trials showed strong BOLD response and are therefore included in the CCEP versus fMRI plots in Figures 5 and 6.
BOLD, blood-oxygen-level-dependent; CCEP, cortico-cortical evoked potential; fMRI, functional magnetic resonance imaging.

P5), and Table 2 gives an overview of the results from every DES-fMRI trial performed. Figure 2 gives the corresponding images of BOLD activation (as measured by the *t*-statistic) for the patients P1 through P4 using high-current (8 or 15 mA) stimulation runs; the second column of Table 2 indicates which image corresponds to which trial. An analogous image for all low-current runs is provided in Figure 3. Patient P5 focused on studying an event paradigm. The *t*-statistic maps in Figures 2 and 3 have a threshold of $|t|>2.6$, which corresponds to a significance level of $p<0.01$.

P1 in Figure 2 shows robust BOLD activation in patient 1, whose extensive workup suggested a left medial orbitofrontal EZ. Figure 2A demonstrates stimulation at the EZ, showing widespread BOLD activation, proximally including the left hippocampus and lateral orbitofrontal lobe. More distally, the pattern of positive activation along the left cingulate suggested activation of the underlying limbic network. In addition to positive BOLD activation, there was negative BOLD activation, including possible underlying network involving the bilateral motor strips, and a large cluster in the contralateral mesial temporal lobe. The magnitude of the BOLD response was robust, with a maximal signal variation of nearly 4% (in a single voxel). Similar to P1, P2 shows exuberant activation with stimulation near the EZ of the medial right frontoparietal lobe, notably including positive and negative activation (Fig. 2D). The negative activation appears more symmetrically and strongly involves the primary cortex of the sensorimotor and visual regions. In P2, there is markedly less activation when stimulation is moved to presumably normal cortex of the lateral left frontoparietal region (Fig. 2E). This pattern is seen to a lesser extent in P1 as stimulation is moved away from the hypothesized EZ; local and network activation remain in Figure 2B but disappear in Figure 2C. P3 shows robust local and distal activation, with relatively no negative activation (Fig. 2F). A markedly different and lesser pattern is seen when the stimulating

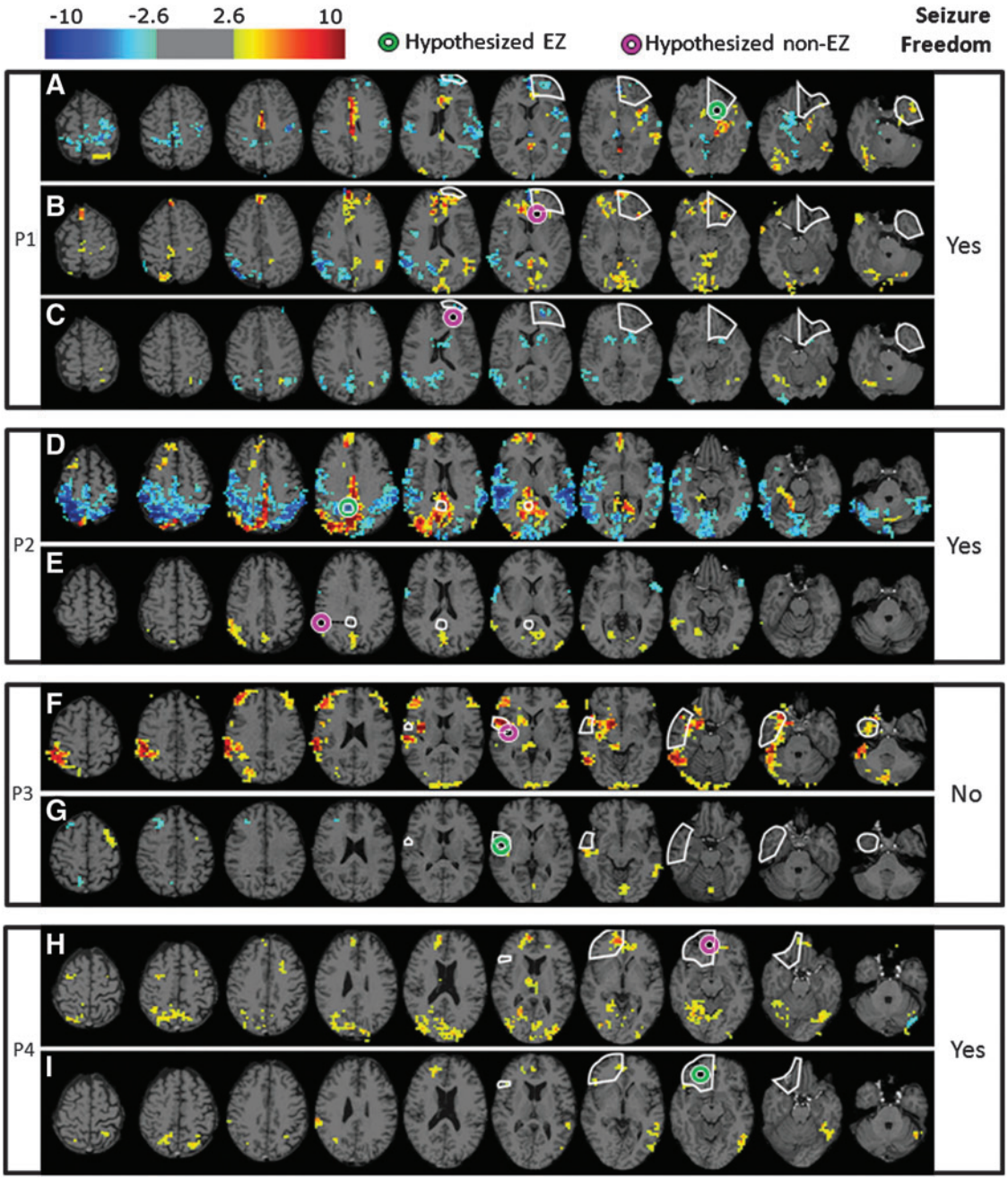

FIG. 2. Compilation of fMRI activation maps for all high-current stimulation trials (All MRI images in this and subsequent figures follow radiological convention, with the patient's left being in the right of the image.). The activation shown is of the *t*-statistic, above a threshold of $|t| > 2.6$ ($p < 0.01$). The site of stimulation in each panel is indicated by a color target; green represents the hypothesized epileptogenic zone (EZ), while magenta represents the control. The region outlined in white shows the area of the brain that was surgically resected. The patient's clinical information and stimulation parameters for each panel are summarized in Tables 1 and 2. P1, P2, P3, and P4: patients 1–4, respectively. Seizure freedom indicates whether or not the patient was free of seizures 6 months after resection. Color images available online at www.liebertpub.com/brain

electrode contacts are moved laterally about 15 mm (Fig. 2G). This pattern actually shows higher levels of activation when stimulated outside the area that was later resected. However, this patient did not remain seizure-free after resection (further discussed in ''BOLD Response Versus Results of Surgery'' section). In P4, we also saw decreased activation when stimulation was moved laterally. In this patient, both stimulation points ended up being contained within the area of resection.

Figure 4 shows an example of the raw MRI signals, derived from P1 in Figure 2, which is averaged over the limbic area (positive activation) and the left motor strip (negative activation), in relation to the blocks of stimulation. The displayed signal variation is not as high as the maximal variation seen in some individual voxels (up to 4%) because it is averaged over multiple voxels, but we can still see a clear response to the stimulation.

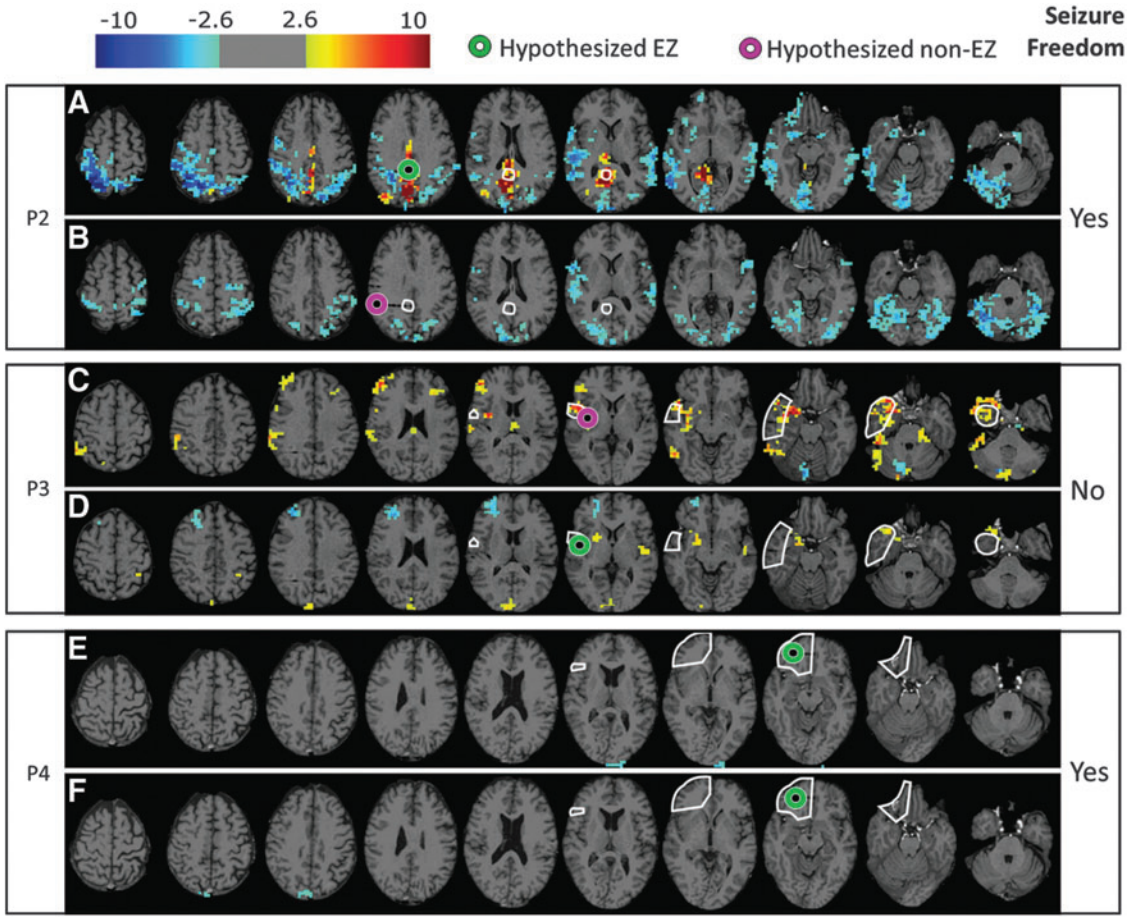

FIG. 3. Compilation of all low-current or low-frequency fMRI activation maps, for patients P2, P3, and P4 (image right = patient's left). Similar to Figure 2, the activation shown is the *t*-statistic, above a threshold of $|t| > 2.6$ ($p < 0.01$). The site of stimulation in each panel is indicated by a color target; green represents the hypothesized EZ, while magenta represents the control. The region outlined in white shows the area of the brain that was surgically resected. The patient's clinical information and stimulation parameters for each panel are summarized in Tables 1 and 2. Seizure freedom indicates whether or not the patient was free of seizures 6 months after resection. Color images available online at www.liebertpub.com/brain

Distal activation in this patient was generated by stimulating not only cortical gray matter but also deep and subcortical white matter, as shown in Figure 2B. Using the same stimulation parameters on an electrode pair located more laterally in the deep white matter, activation clearly extended to the contralateral side, likely propagating along fibers of the anterior corpus callosum. Robust contralateral negative activation was also seen in the right inferior parietal lobule. With these scans, we demonstrated that DES-fMRI can generate robust BOLD activation throughout the brain, in proximal, distal, and interhemispheric regions.

Comparison to CCEP

Measures of CCEP response strength were compared to fMRI *t*-statistics in voxels coregistered to recording

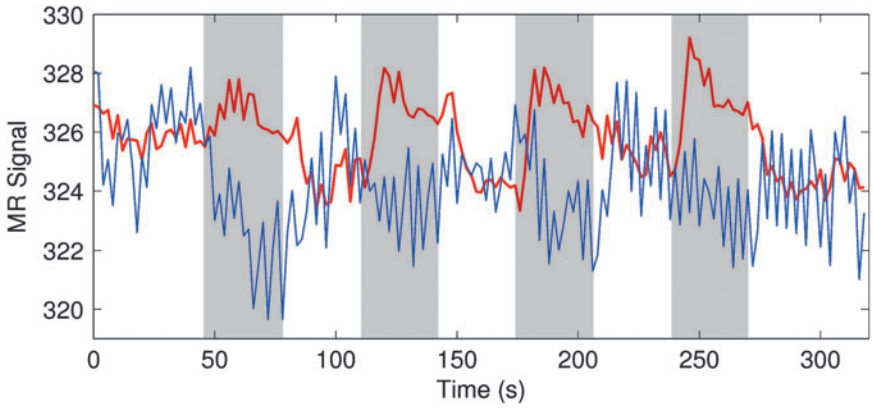

FIG. 4. Raw MR signals in patient P1. The thick red curve shows the MR signal averaged over the positively activated voxels of the limbic area in Figure 2A. The thin blue curve shows the MR signal averaged over the negatively activated voxels in the left motor strip in Figure 2A. Sections shaded in gray indicate the times when stimulation was on (15 mA, 20 Hz). Color images available online at www.liebertpub.com/brain

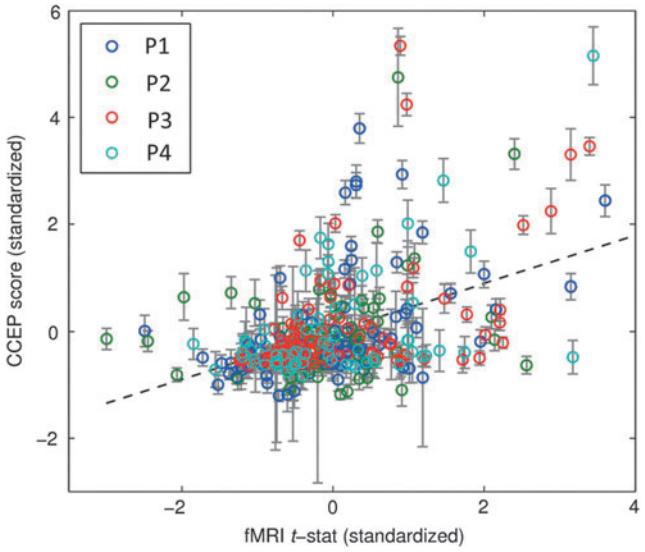

FIG. 5. CCEP response versus fMRI response to stimulation. The CCEP score at each recording contact is plotted against the fMRI *t*-statistic in the coregistered voxel. Different colors represent different trials/patients. The trials included in the plot, along with a summary of the parameters used, are indicated in Table 2 by an asterisk (*). CCEP and fMRI scores are standardized for each trial to account for differences in the ranges of scores observed. Error bars represent the standard deviation of the CCEP recordings used to produce the average waveforms. The dashed line shows the least squares line of best fit. Color images available online at www.liebertpub.com/brain

electrode contacts. Figure 5 shows the correlation for all four high-current trials (one from each patient) that produced a robust BOLD response (indicated with a [*] in the seventh column of Table 2). Each data point represents the localized CCEP response around a recording electrode and fMRI activation in the corresponding voxel. The CCEP and fMRI scores from these four trials were standardized for each patient (to account for differences in ranges of scores observed) and combined to compute an overall correlation coefficient. The overall correlation observed was significant and positive (Pearson's $r=0.45$; $p=1.9\times10^{-17}$; $n=326$). CCEP versus fMRI correlations for individual trials are shown in the sixth column of Table 2. Single-trial correlations were as high as $r=0.54$ ($p=2.8\times10^{-9}$; $n=106$), but fMRI trials with weaker BOLD statistics generally showed poorer correlations. One trial (Table 2, row 7) showed a significant negative correlation; note that this trial also showed a weak BOLD response, which may increase sensitivity to error. Figure 6 shows an analysis of the same data as Figure 5, but using different mathematical methods to derive a CCEP score, specifically by using peak-to-peak amplitudes rather than root mean square (refer to Fig. 1). A similar result to Figure 5 is obtained using either of two possible peak-to-peak measures, again demonstrating a significant but weak correlation.

Effects of different experimental parameters

The magnitude of BOLD activation was heavily frequency dependent. As mentioned in the ''Materials and Methods'' section, the first three patients in the study were stimulated at 1 Hz and showed no significant ($p<0.01$, $|t|>2.6$) BOLD response. Robust activation was always seen at 20 Hz in subsequent patients, but reducing the frequency to 10 or 5 Hz led to no significant activity above the same threshold (Table 2: right pars orbitalis stimulation in P4).

The activation generated with different stimulation currents appeared to have similar patterns but differing magnitudes in response strength. For example, Figures 2D and 3A show the high- and low-current fMRI activation, respectively, in a patient with a hypothesized EZ in the medial right parietal lobe. The activation patterns are very similar, with the high-current stimulation simply showing greater spread. In one

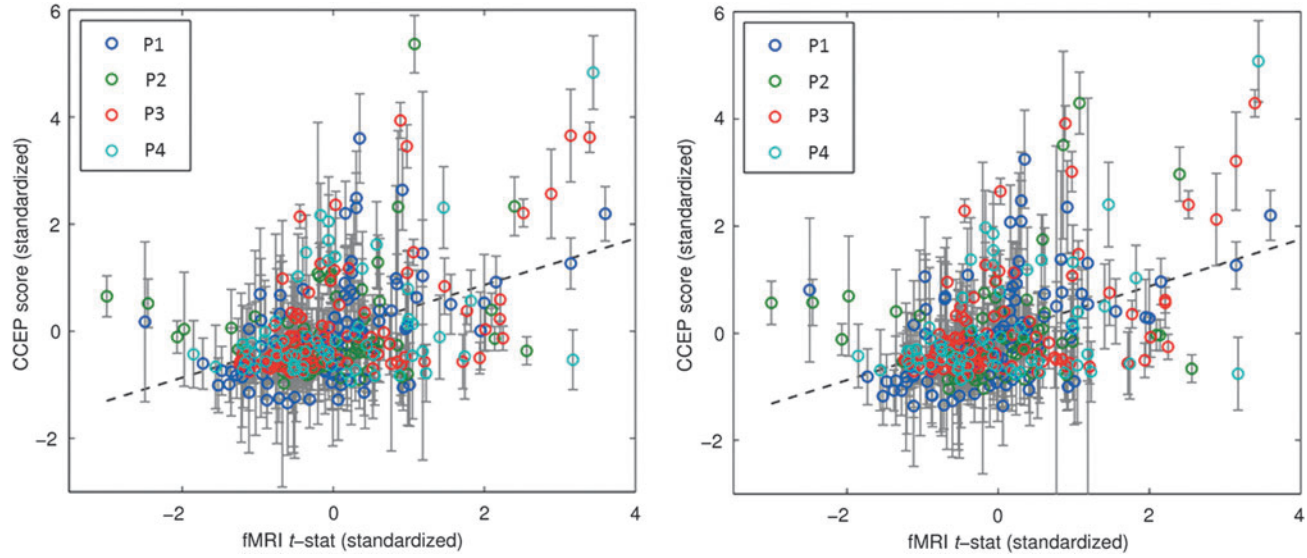

FIG. 6. CCEP response versus fMRI response to stimulation, using peak-to-peak scoring of CCEPs. The plots above show the same data as Figure 5, but the CCEPs are scored using peak-to-peak amplitudes rather than root-mean-square (see Fig. 1). The panel on the left uses the first peak-to-peak amplitude ($r=0.43$; $p=2.6\times10^{-16}$; $n=326$), while the panel on the right uses the second peak-to-peak amplitude ($r=0.44$; $p=9.7\times10^{-17}$; $n=326$). Color images available online at www.liebertpub.com/brain

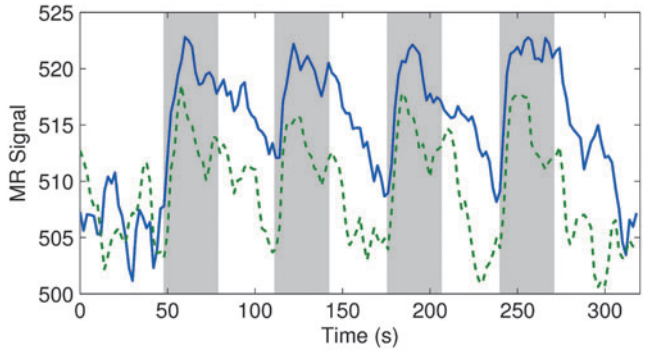

FIG. 7. Averaged positive blood-oxygen-level-dependent (BOLD) response in patient P2. Activation was generated at 4 mA (green, dashed) and 8 mA (blue, solid) stimulation. The *y*-axis shows the MR signal averaged over all voxels with $t > 3$ in both low- and high-current runs. Sections shaded in gray represent the times when the stimulation was on. Color images available online at www.liebertpub.com/brain

location of stimulation, we observed a mostly positive response at high current (Fig. 2E) and a mostly negative response at low current (Fig. 3B). This was the only paired high–low-current stimulation to show this pattern and needs to be further investigated. We correlated the fMRI *t*-values resulting from all of the corresponding low-current and high-current trials in Table 2 (subjects P2 and P3), considering only voxels in the brain volume. The resulting Pearson's *r* coefficient ($n = 37{,}196$ voxels across four trials) was $r = 0.48$.

Regarding the magnitudes in BOLD response, Figure 7 (taken from the same trials as Figs. 2D and 3A) shows that the average change of MR signal in activated voxels was greater for high current (8 mA; ~3.6%) than for low current (4 mA; ~2.6%). The signal also took longer to return to baseline after the end of stimulation for high current than for low. Despite the difference in signal change, the BOLD response was robust for both the 4- and 8-mA runs.

Figure 8 shows examples of CCEPs recorded in patient P2 with and without anesthesia. Stimulation occurred in the right superior temporal gyrus. Most recording contacts (134 out of 140) demonstrated only minimal differences in voltage signals within the first 50 msec and moderate differences thereafter. The remaining six contacts showed significant differences. Stimulation in other locations and other patients showed similar trends. We correlated the anesthetized and nonanesthetized CCEP responses at each recording contact and each time point (300 time points per contact, at 1 kHz sampling over the first 0.3 sec), for all trials (two patients, two locations each) in which we performed CCEPs with and without anesthesia. The resulting Pearson's *r* coefficient ($n = 144{,}232$ time points over four trials) was $r = 0.85$.

Block design versus event design

In addition to a block design, event-related paradigms were obtained for a direct comparison shown in Figure 9, which was the most successful in patient P5 after increasing the stimulation duration from 1 to 2 sec, which was used in the previous patients. The top panel shows the event design and the bottom panel shows a corresponding block design (both using 8 mA and 20 Hz stimulation pulses). The location of stimulation was in the hypothesized EZ located in the right anterior insula, which is visualized as the location of maximal response in each case. There is a remarkable similarity in the patterns of the activation maps derived from the block design and the event design, with a difference mainly in magnitude. This similarity is reassuring between the two major methodologies, and shows the future potential of optimizing the event paradigm as a method to probe the temporal-spatial dynamics of the evolving BOLD response, whereas the block paradigm can only probe the spatial patterns. An example of the need to further explore the parameters of the event paradigm is that a similar but far weaker correspondence was seen in two earlier patients where the event stimulation was attempted with stimulation duration of 1 sec (not shown).

BOLD response versus results of surgery

Note that all surgical resections were planned and performed based on routine clinical decision making; specifically, the

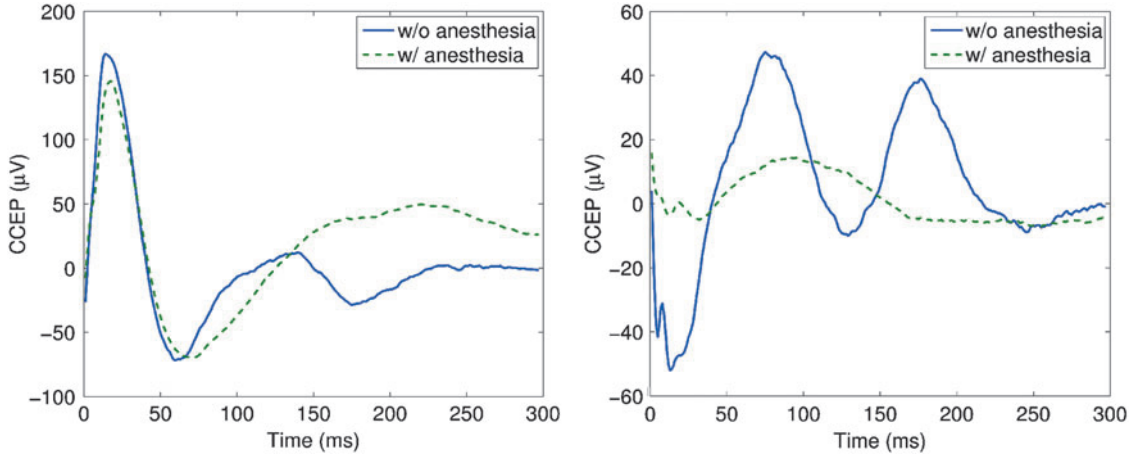

FIG. 8. Effect of anesthesia on CCEPs. Shown are CCEP recordings at two electrode contacts, taken from a trial on patient P2 without (blue, solid) and with (green, dashed) anesthesia. The contact on the left shows a small effect of anesthesia representative of most recording contacts (134/140). The panel on the right shows a larger effect of anesthesia, but this was observed in very few recording contacts (6/140). Color images available online at www.liebertpub.com/brain

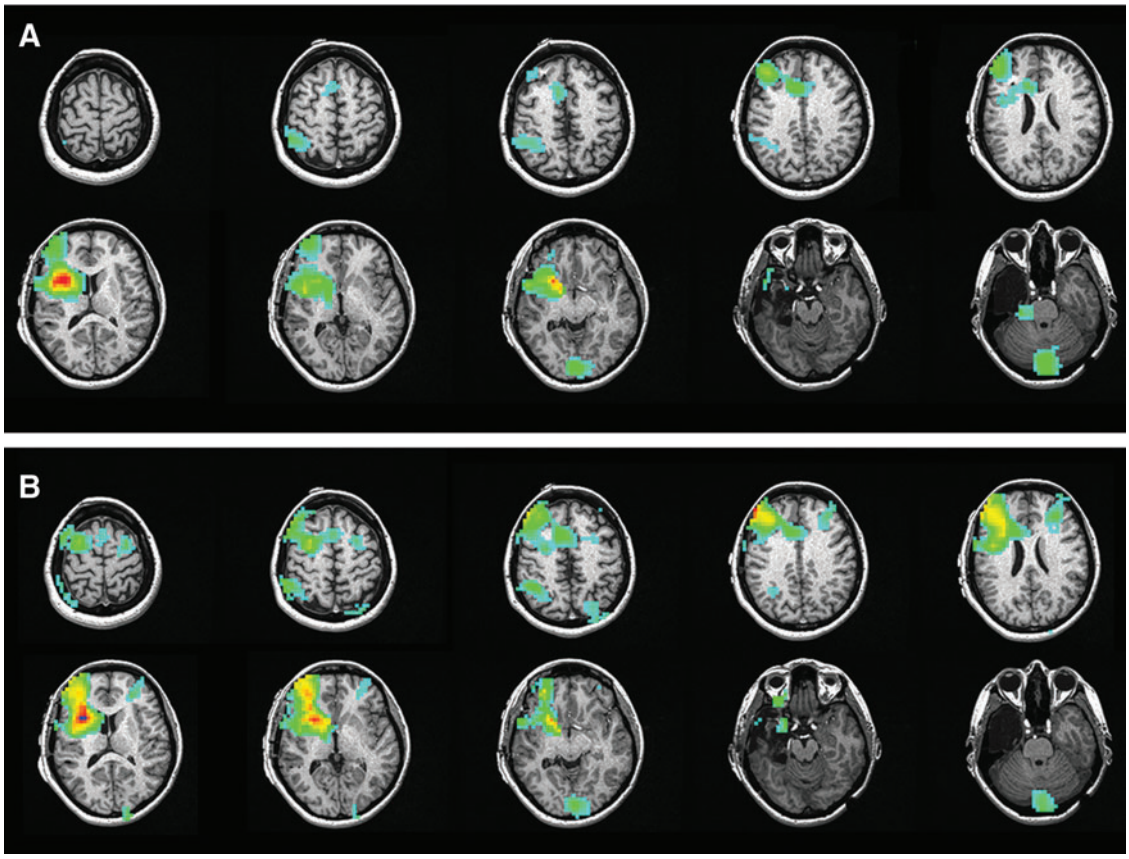

FIG. 9. Event versus block stimulation paradigm (image right = patient's left). The top panel **(A)** shows the event design applied a hypothesized EZ in the right anterior insula, using a stimulation lasting 2 sec (8 mA at 20 Hz), followed by 11 sec of rest. The bottom panel **(B)** shows images from the same patient with application of a corresponding block design, also at 8 mA and 20 Hz. In both cases there is a display threshold of $t = 3$, and the maximum color is $t = 9$. Only positive activation is shown for clarity. Color images available online at www.liebertpub.com/brain

margins were not influenced by the BOLD maps obtained during this study. Table 2 shows that three out of four patients (P1, P2, and P4) remain seizure free after undergoing surgery. In all three of these patients, the surgeon resected the area of the brain that elicited strong local BOLD activation when stimulated. In two of these three patients (P1 and P2), the area of the brain that elicited strong local BOLD response was the *only* stimulated area that was resected (in P4, both stimulation areas were resected). On the other hand, the patient who relapsed into seizures (P3) was the only one who did not have the area that elicited strong local BOLD response resected. In theory, we would expect epileptic areas of the brain to display a stronger local BOLD response when stimulated, because epileptic tissue is more easily excited, as suggested by earlier results from CCEP studies (Iwasaki et al., 2010). However, this is only a preliminary observation; we need a larger sample size to make any conclusions about DES-fMRI predicting the success of surgery.

Discussion

In this study, we found that DES-fMRI produces robust networks of BOLD activation that show a significant positive correlation with electrical recordings. These results suggest that DES-fMRI could be used for full-brain-volume evaluation in studies of brain connectivity, including surgical planning for patients with medically intractable epilepsy.

We pose the following mechanism for DES-fMRI activation; the initiating event is depolarization of axons within some volume surrounding the stimulating electrode contacts, caused by an impressed and altered extracellular potential along the axonal membranes. This activation function alters the membrane potential to either depolarized or hyperpolarized depending on the geometry and polarity of the stimulating electrodes relative to the membrane (Joucla and Yvert, 2012; McIntyre et al., 2004; Rattay, 1999). If sufficiently strong, then foci of depolarization cause local action potentials, which then propagate not only locally but also distally to regions far outside the stimulation zone, as also seen in recent animal experiments (Lai et al., 2014). It is unclear how this propagation might be affected within the volume of the stimulation zone, where other axonal pathways have likely depolarized and may be refractory to propagation, in addition to having inhibitory circuits excited. More distally, if a shower of efferent action potentials can cause remote cortical processes to trigger a sufficient collective response, then the resulting altered local field potential can be detected by two mechanisms: (1) adjacent electrodes measuring the local field potential manifest as an increased CCEP response

(Logothetis, 2003), and (2) assuming a tight relationship of neurovascular coupling, then induced increased cerebral blood flow manifests as an increased BOLD response (Logothetis, 2003).

Limitations and uncertainties

Although the overall correlation (across four trials in four different patients with correlative data) between CCEP score and fMRI activation was significant (Figs. 5 and 6), there were many locations in the brain with strong CCEP response but weak BOLD response and vice versa. One major technical reason could be inaccuracy regarding the exact origin of the CCEP signal, which in this analysis was assumed to be exactly colocalized with the electrode contacts. Since the uncertainty is likely comparable to the spacing between electrode contacts (about 5 mm) (Juergens et al., 1999; Logothetis, 2003), the scatter plots may have compared CCEP and BOLD values not from colocalized voxels, but from locations that are up to two to three voxels apart. The variation in BOLD activation over this distance could have contributed to a poor correlation. Imperfect registration of the CCEP electrode contacts to the fMRI volume could also weaken the correlation. A related source of error is the choice of reference for CCEPs, since the ability to measure electrophysiological activity depends on the relative positioning between the recording contact, reference, and depolarized tissue. The imperfect localization of activated sources is actually an inherent weakness of CCEPs that can be augmented by fMRI.

Another limitation of the comparison—and a possible explanation for the imperfect correlation—is that the stimulation paradigm used for fMRI differs from the CCEP protocol performed outside the MR scan. Low-frequency (1 Hz) stimulation was used outside the MR scan to follow standard clinical protocols for CCEP evaluation, whereas the stimulation used during MRI required a higher frequency to elicit a BOLD response (typically 20 Hz). Thus, differences in the CCEP-BOLD correlation may have been secondary to frequency-dependent patterns of BOLD/CCEP response. In future experiments, CCEPs will also be performed at 20 Hz to make a congruent comparison to the 20-Hz stimulation during fMRI.

From Table 2, we can see that the CCEP-fMRI correlation is moderate for the six acquisitions producing a strong BOLD response, with a mean value of 0.38. Note that almost all of the trials with poor correlation also showed weak BOLD activation. Therefore, the weak correlation of those individual trials could be a result of the uncertainty associated with the weak fMRI statistics being used to correlate with CCEPs. Of the trials that showed a strong BOLD response, each one showed a positive correlation between CCEPs and BOLD with $p < 0.05$, except for the 4-mA stimulation of the right posterior cingulate in patient P2 (Fig. 3A). One feature in our results so far is the difference in the strength of BOLD response across different locations of stimulation. As we can see from Figure 2, trials in the same patient, using the same stimulation parameters, can elicit different strengths of response depending on which area of the brain was stimulated. We do not know the cause of this difference in response strength. Although one possible reason is intrinsically different BOLD reactivity to DES in different regions of the brain, a far more intriguing possibility is that the variation can reflect underlying epileptogenicity. That is, stimulating an area that is more prone to spreading discharges (i.e., near or within the EZ) produces a more robust BOLD response than stimulating an area far from the EZ, even if using the same stimulation parameters. This concept could be extended further to speculate that stimulating within the ''epileptogenic network'' (but outside the seizure onset zone) would also elicit a more intense BOLD response than outside this ''network,'' but less intense than the stimulation within the seizure onset zone (a ''gradient'' of response that could perhaps help in mapping the EZ). A future plan is to explore the range of stimulation frequency and current more thoroughly, and to examine how responses differ depending on the location stimulated.

Another uncertainty regards the effects of anesthesia. Since these experiments were conducted as a ''piggy back'' to a standard neurosurgical procedure, there was only limited control of the exact choice and dose of anesthetics. This accounts for the variability of injected concentrations and inhaled agents mentioned in the ''Materials and Methods'' section. Future work would entail more systematic study of anesthetic agents on both the CCEPS and fMRI responses. Such an investigation would be more efficient with the use of an animal model.

The observation of ''negative activation'' is noteworthy, since it appears directly as a result of positive stimulation. Negative activation is often seen in fMRI with awake patients using a block paradigm, and is likely a feature of the paradigm design wherein the presumed rest condition is actually not rest. That is, even at ''rest'' a subject's brain is rarely doing nothing, and is likely active in some state, for example, the default mode network, which is then suppressed during a task and appears as negative activation from the fMRI analysis methods. These results are further confounded by any volitional influence by subjects during the resting state. Conversely, in these experiments, the patient is unconscious and there is no volitional modulation of the resting state. This does not discount the possibility of a reflexive nature to the change of resting state due to stimulation, which does not require consciousness.

Clinical applications

The driving application for these experiments is improved identification and anatomical delineation of the EZ, which can increase the surgical cure rate of patients with pharmacoresistant focal seizures. One limitation of invasive evaluation is incomplete parenchymal coverage. Subdural grids cover only the surface of the brain, and depth electrodes sample only thin cylindrical sections of brain volume (Behrens et al., 1994). Therefore, if the surgeon does not place electrodes close enough to the hypothetical EZ, the resulting data may be insufficient to locate this area. This possibility may result in a significant number of early postoperative failures (Najm et al., 2013). Since the BOLD response was shown to be consistent with electrical recordings, the complete coverage and precise localization of fMRI could be used to complement invasive evaluation. Specifically, DES-fMRI can extend the range of CCEP evaluation to the entire brain. The DES-fMRI technique may also improve the yield of invasive evaluations by identifying regions of

the brain with high activity that warrant sampling of an SEEG electrode. This procedure could be performed intraoperatively and interactively, with the DES-fMRI data from each SEEG electrode informing placement of the next electrode.

There are also two direct potential applications of DES-fMRI to identification of the EZ. The first extends an observation from clinical CCEPs demonstrating accentuated local voltage response to stimulation of the EZ (when compared with stimulation of normal tissue) (Iwasaki et al., 2010). As suggested in ''Block Design Versus Event Design'' section, there may be a parallel phenomenon in DES-fMRI showing enhanced local BOLD response during stimulation of the EZ. As we obtain results from more patients, these activation magnitudes could be compared with those derived from stimulation of normal tissue at the same location in an ensemble of prior patients. A second method for identification of the EZ would add spontaneous electroencephalography-correlated fMRI (EEG-fMRI) (Cunningham et al., 2012; Gotman, 2008), whose patterns of activation represent a signature of the causative endogenous interictal discharges. If a stimulated DES-fMRI pattern can match the endogenous EEG-fMRI pattern, the location of active stimulation likely coincides with the location of the endogenous source.

Although the presented results are compelling, many questions still need to be answered. Further studies are required to compare the activation patterns with respect to stimulating the EZ versus stimulating non-EZ regions. Further studies also need to address variation of results depending on which region of the brain was stimulated. In this study, we observed how certain experimental parameters, such as stimulation frequency and current, can affect the BOLD response; these results will guide further experiments devoted to optimizing the stimulation and fMRI acquisition parameters. The exact clinical relevance of our BOLD activation maps also needs to be determined. Long-term studies assessing clinical outcomes, pathology, and activation maps are needed to assess the value of DES-fMRI data. By comparing pathology and clinical outcomes with DES-fMRI data, we hope to find features in the data that are correlated with successful surgery.

Table 3. Summary of Main Observational Results from Direct Electrical Stimulation–Functional Magnetic Resonance Imaging

1. Strong regional and distal BOLD activation can be induced by block design intracranial electrical stimulation.
2. Patterns of activation suggest underlying physiologic networks.
3. Both positive and negative activation are induced.
4. Stimulation of both white matter and gray matter can cause activation.
5. Results are dependent on stimulation frequency for a block design.
6. High and low currents induce similar activation patterns, but higher currents show greater spread.
7. In trials with strong BOLD response, there is a significant correlation of BOLD response to corresponding electrophysiological response.
8. Postoperative pathological specimens showed no thermal damage.
9. Effects of used general anesthetic agents and doses on intracranial-stimulation-evoked electrophysiological response are very small.
10. Event design triggers BOLD response with 2-sec stimulation, and reveals temporal spread pattern, showing both rapid and slow components.

Conclusions

In summary, our results show that direct electrical stimulation with fMRI BOLD mapping leads to an activation of large well-mapped functional networks as mapped by CCEPs. In addition significant correlations were found between BOLD, epileptic regions, and evoked potential responses. Our conclusion with regards to stimulation parameters is that high-frequency stimulation (20 Hz) at 4 or 8 mA in a block design gives the most robust BOLD response. Event paradigm stimulation can yield a similar BOLD response and may elucidate temporal patterns of how activation spreads. The utility of event design stimulation and additional exploration of stimulation parameters remains to be studied further in future work. A list of our main conclusions can be found in Table 3.

Acknowledgments

The authors thank Karl Horning for help with testing electronics, Katie Murphy for scheduling patients, Megan Griffiths for reviewing the article, and John Gale for helpful discussions on stimulation techniques. We thank grant support from Citizens United for Research in Epilepsy (CURE1201SJ).

Author Disclosure Statement

No competing financial interests exist.

References

Angenstein F, Kammerer E, Niessen HG, Frey JU, Scheich H, Frey S, et al. 2007. Frequency-dependent activation pattern in the rat hippocampus, a simultaneous electrophysiological and fMRI study. Neuroimage 38:150–163.

Baker KB, Tkach JA, Nyenhuis JA, Phillips M, Shellock FG, Gonzalez-Martinez J, et al. 2004. Evaluation of specific absorption rate as a dosimeter of MRI-related implant heating. J Magn Reson Imaging 20:315–320.

Baker KB, Tkach JA, Phillips MD, Rezai AR. 2006. Variability in RF-induced heating of a deep brain stimulation implant across MR systems. J Magn Reson Imaging 24:1236–1242.

Behrens E, Zentner J, van Roost D, Hufnagel A, Elger CE, Schramm J. 1994. Subdural and depth electrodes in the presurgical evaluation of epilepsy. Acta Neurochir 128: 84–87.

Berg AT. 2009. Identification of pharmacoresistant epilepsy. Neurol Clin 27:1003–1013.

Berg AT, Kelly MM. 2006. Defining intractability: comparisons among published definitions. Epilepsia 47:431–436.

Brodie MJ, Shorvon SD, Canger R, Halász P, Johannessen S, Thompson P, et al. 2005. Commission on European affairs: appropriate standards of epilepsy care across Europe. Epilepsia 38:1245–1250.

Cox RW, Hyde JS. 1997. Software tools for analysis and visualization of fMRI data. NMR Biomed 10:171–178.

Cunningham CB, Goodyear BG, Badawy R, Zaamout F, Pittman DJ, Beers CA, et al. 2012. Intracranial EEG-fMRI analysis of

focal epileptiform discharges in humans. Epilepsia 53:1636–1648.
Gordon B, Lesser RP, Rance NE, Hart J, Jr., Webber R, Uematsu S, et al. 1990. Parameters for direct cortical electrical stimulation in the human: histopathologic confirmation. Electroencephalogr Clin Neurophysiol 75:371–377.
Gotman J. 2008. Epileptic networks studied with EEG-fMRI. Epilepsia 49:42–51.
Hesselmann V, Sorger B, Girnus R, Lasek K, Maarouf M, Wedekind C, et al. 2004. Intraoperative functional MRI as a new approach to monitor deep brain stimulation in Parkinsons disease. Eur Radiol 14:686–690.
Iwasaki M, Enatsu R, Matsumoto R, Novak E, Thankappen B, Piao Z, et al. 2010. Accentuated cortico-cortical evoked potentials in neocortical epilepsy in areas of ictal onset. Epileptic Disord 12:292–302.
Jayakar P. 1993. Physiological principles of electrical stimulation. Adv Neurol 63:17–27.
Jech R, Urgosík D, Tintera J, Nebuzelský A, Krásenský J, Liscák et al. 2001. Functional magnetic resonance imaging during deep brain stimulation: a pilot study in four patients with Parkinson's disease. Mov Disord 16:1126–1132.
Jenkinson M, Bannister PR, Brady JM, Smith SM. 2002. Improved optimisation for the robust and accurate linear registration and motion correction of brain images. NeuroImage 17:825–841.
Jenkinson M, Smith SM. 2001. A global optimisation method for robust affine registration of brain images. Med Image Anal 5:143–156.
Joucla S, Yvert B. 2012. Modeling extracellular electrical neural stimulation: from basic understanding to MEA-based applications. J Physiol Paris 106:146–158.
Juergens E, Guettler A, Eckhorn R. 1999. Visual stimulation elicits locked and induced gamma oscillations in monkey intracortical-and EEG-potentials, but not in human EEG. Exp Brain Res 129:247–259.
Kwan P, Brodie MJ. 2000. Early identification of refractory epilepsy. N Engl J Med 342:314–319.
Lai H, Younce J, Albaugh D, Kao Y, Shih Y. 2014. Functional MRI reveals frequency-dependent responses during deep brain stimulation at the subthalamic nucleus or internal globus pallidus. Neuroimage 84:11–18.
Lesser RP, Lüders HO. 1987. Extraoperative cortical functional localization in patients with epilepsy. J Clin Neurophysiol 4:27–53.
Logothetis NK. 2003. The underpinnings of the BOLD functional magnetic resonance imaging signal. J Neurosci 23: 3963–3971.
Logothetis NK. 2012. Intracortical recordings and fMRI: an attempt to study operational modules and networks simultaneously. Neuroimage 62:962–969.
Matsui T, Tamura K, Koyano KW, Takeuchi D, Adachi Y, Osada T, et al. 2011. Direct comparison of spontaneous functional connectivity and effective connectivity measured by intracortical microstimulation: an fMRI study in macaque monkeys. Cereb Cortex 21:2348–2356.
Matsumoto R, Nair DR, LaPresto E, Bingaman W, Shibasaki H, Lüders HO. 2007. Functional connectivity in human cortical motor system: a corticocortical evoked potential study. Brain 130:181–197.
Matsumoto R, Nair DR, LaPresto E, Najm I, Bingaman W, Shibasaki H, et al. 2004. Functional connectivity in the human language system: a corticocortical evoked potential study. Brain 127:2316–2330.
McIntyre CC, Grill WM, Sherman DL, Thakor NV. 2004. Cellular effects of deep brain stimulation: model-based analysis of activation and inhibition. J Neurophysiol 91:1457–1469.
Modica PA, Tempelhoff R, White PF. 1990. Pro-and anticonvulsant effects of anesthetics (Part II). Anesth Analg 70:433–434.
Najm I, Jehi L, Palmini A, Gonzalez-Martinez J, Paglioli E, Bingaman W. 2013. Temporal patterns and mechanisms of epilepsy surgery failure. Epilepsia 54:772–782.
Phillips MD, Baker KB, Lowe MJ, Tkach JA, Cooper SE, Kopell BH, et al. 2006. Parkinson disease: pattern of functional MR imaging activation during deep brain stimulation of subthalamic nucleus—initial experience. Radiology 239:209–216.
Rattay F. 1999. The basic mechanism for the electrical stimulation of the nervous system. Neuroscience 89:335–346.
Rezai AR, Finelli D, Nyenhuis JA, Hrdlicka G, Tkach J, Sharan A, et al. 2002. Neurostimulation systems for deep brain stimulation: in vitro evaluation of magnetic resonance imaging-related heating at 1.5 tesla. J Magn Reson Imaging 15:241–250.
Sillanpää M, Schmidt D. 2006. Natural history of treated childhood-onset epilepsy: prospective, long-term population-based study. Brain 129:617–624.
Stefurak T, Mikulis D, Mayberg H, Lang AE, Hevenor S, Pahapill P, et al. 2003. Deep brain stimulation for Parkinsons disease dissociates mood and motor circuits: a functional MRI case study. Mov Disord 18:1508–1516.
Tolias AS, Sultan F, Augath M, Oeltermann A, Tehovnik EJ, Schiller PH, et al. 2005. Mapping cortical activity elicited with electrical microstimulation using FMRI in the macaque. Neuron 48:901–911.

Address correspondence to:
Stephen E. Jones
Imaging Institute, U-15
Cleveland Clinic
9500 Euclid Avenue
Cleveland, OH 44195

E-mail: joness19@ccf.org